

1-30-2013

Numerical simulation of traffic flow using a hydrodynamic model

Craig VanderPloeg

Follow this and additional works at: https://digitalrepository.unm.edu/math_etds

Recommended Citation

VanderPloeg, Craig. "Numerical simulation of traffic flow using a hydrodynamic model." (2013). https://digitalrepository.unm.edu/math_etds/50

This Thesis is brought to you for free and open access by the Electronic Theses and Dissertations at UNM Digital Repository. It has been accepted for inclusion in Mathematics & Statistics ETDs by an authorized administrator of UNM Digital Repository. For more information, please contact disc@unm.edu.

Craig VanderPloeg

Candidate

Mathematics

Department

This thesis is approved, and it is acceptable in quality and form for publication:

Approved by the Thesis Committee:

Alexander Korotkevich

, Chairperson

Daniel Appelo

Evangelos Coutsias

Deborah Sulsky

Numerical Simulation of Traffic Flow Using a Hydrodynamic Model

by

Craig VanderPloeg

B.S., Mathematics, Michigan State University, 1994

THESIS

Submitted in Partial Fulfillment of the
Requirements for the Degree of

Master of Science
Mathematics

The University of New Mexico

Albuquerque, New Mexico

December, 2012

©2012, Craig VanderPloeg

Dedication

For all who continually work hard through the goal of completion

Acknowledgments

First, I would like to thank Dr. Alexander Korotkevich, for his guidance throughout the development of this paper, for his patience, for being my thesis advisor, and for being the chair of my thesis committee. Gratitude is to be given to Dr. Alexandru Buium for taking the time to listen to my thoughts and for fostering my development as a graduate student. It is my honor to have Dr. Daniel Appelo, Dr. Evangelos Coutsias, and Dr. Deborah Sulsky serve on my thesis committee. I give my appreciation to Galina Watts, for motivating me to become a graduate student, Erik Teixeira, for answering my questions concerning Matlab, David Weirich, for his exceptional knowledge and assistance with L^AT_EX, my longtime friend and companion, Suzanne Rector, for her encouragement and caring heart, and my grandfather, Duane Quigg, for his contributions in helping me complete my degree.

Numerical Simulation of Traffic Flow Using a Hydrodynamic Model

by

Craig VanderPloeg

B.S., Mathematics, Michigan State University, 1994

M.S., Mathematics, University of New Mexico, 2012

Abstract

We examine the solution to the system of partial differential equations for the transport and continuity equations. The model for our system of equations closely resembles the Payne-Whitham model for traffic flow. The solution can be approximated closely through the method of finite differencing. We approach this approximation of the solution through computer simulation in Matlab.

Contents

List of Figures	ix
List of Tables	xi
1 Introduction	1
2 System of Equations	5
2.1 Introducing the Transport Equation	6
2.2 Introducing the Continuity Equation	6
2.3 Solving the System of Equations	7
2.4 Modeling the Right-Hand Side of the Transport Equation	7
2.4.1 Parameters	8
2.4.2 Desired Velocity	9
3 Numerical Scheme	12
3.1 Numerical Scheme for the Transport Equation	13

Contents

3.2	Stability Conditions for the Transport Equation	16
3.3	Error Approximation for the Transport Equation	18
3.4	Numerical Scheme for the Continuity Equation	20
3.5	Stability Conditions for the Continuity Equation	25
3.6	Error Approximation for the Continuity Equation	27
4	Modeling	32
4.1	Traffic Jams and Work Zones	33
4.2	Scenarios	33
4.3	Results of Simulation	36
5	Conclusion	43

List of Figures

1.1	Phantom Traffic Jam	1
2.1	Distance between cars	11
3.1	Schematic representation of our numerical scheme	16
3.2	Transport: Max Error vs. τ	19
3.3	Transport: $\log(\text{Max Error})$ vs. $\log(\tau)$	20
3.4	Transport: Max Error vs. h	22
3.5	Transport: $\log(\text{Max Error})$ vs. $\log(h)$	23
3.6	Continuity: Max Error vs. τ	28
3.7	Continuity: $\log(\text{Max Error})$ vs. $\log(\tau)$	29
3.8	Continuity: Max Error vs. h	30
3.9	Continuity: $\log(\text{Max Error})$ vs. $\log(h)$	31
4.1	High Homogeneous ρ , Sharp Δv Top Left: $t=0.000$; Top Right: $t=0.004$; Bottom Left: $t=0.015$; Bottom Right: $t=0.100$	37

List of Figures

4.2	High Homogeneous ρ , Smooth Δv Top Left: $t=0.000$; Top Right: $t=0.009$; Bottom Left: $t=0.031$; Bottom Right: $t=0.100$	38
4.3	High Inhomogeneous ρ , Sharp Δv Top Left: $t=0.000$; Top Right: $t=0.018$; Bottom Left: $t=0.030$; Bottom Right: $t=0.055$	40
4.4	High Inhomogeneous ρ , Smooth Δv Top Left: $t=0.000$; Top Right: $t=0.021$; Bottom Left: $t=0.040$; Bottom Right: $t=0.060$	41
4.5	Low Homogeneous ρ , Sharp Δv Top Left: $t=0.000$; Top Right: $t=0.002$; ■ Bottom Left: $t=0.014$; Bottom Right: $t=0.031$	42

List of Tables

3.1	Transport Equation Errors, τ vs. N	21
3.2	Transport Equation Errors, h vs. N	21
3.3	Continuity Equation Errors, τ vs. N	30
3.4	Continuity Equation Errors, h vs. N	30
4.1	Table of Parameters for Simulations	34

Chapter 1

Introduction

Our investigation into the flow of traffic leads us to describe the behavior of velocity and density of traffic in terms of waves. And so, these waves of traffic lead us to our hydrodynamic model. The study of traffic flow has become a rich topic of current research in both physics and mathematics.

Figure 1.1: Phantom Traffic Jam



Chapter 1. Introduction

A collaborative research group at MIT currently has a website that presents theoretical results concerning specific wave solutions of continuum traffic models. Their research is summarized in an article where they describe how traffic models behavior similar to the equations of fluid flow. They describe how instabilities of traffic flow are observed to grow into traveling waves by modeling the behavior of traffic on a closed, circular track. They also explain how at low densities, traffic may behave nicely. Whereas, at a critical density, traffic becomes unstable, and small disturbances amplify, growing into traveling waves (which we also shall see in our discussion). These incidents lead into what they consider “phantom traffic jams” and “jamitons” (as an analogy to other traveling waves, “solitons”). When many jamitons occur this can lead to behavior in traffic flow similar to what we see in detonation theory, such as “traveling roll waves”. Then, this in turn, can lead to highly complex traffic behavior. The traffic model they use is similar to what we will be using in our thesis. Of particular interest is what transpires when instabilities occur in this system [4].

A new presence in the study of traffic flow is the “intelligent car”. These are cars not entirely operated by people. Essentially, these cars are equipped with sensors and intervehicular communications systems. With sensors and adaptive cruise control (ACC), highway capacity could increase by a factor of 1.4 to 3.7. Smarter cars could also mean less traffic congestion and the ability of cars to drive on their own (through ACC) [1].

Equipping cars with new technology, such as sensors and vehicle-to-vehicle (v2v) communication, may make the car aware of other cars on the road and road conditions, and may also help in the avoidance of collisions. In turn, this may also lead to saving a driver’s money and life. With the evolution of these new types of technology and phenomena, the result may be a dramatic change of the number of cars on the road, as well as, the density of cars on the road (in terms of a noticeable increase)

Chapter 1. Introduction

[9].

In another related topic of traffic flow we can see how congestion on the internet affects network efficiency similar to the way busy roads during rush hour can affect the efficiency of traffic. Researchers from the Chinese Academy of Sciences in Beijing in a recent paper discuss different strategies of network efficiency, including how developing better routing strategies and optimizing the network itself can help in increasing an internet's transmission efficiency. These strategies may cross-over into helping areas of biology, sociology (like transportation or traffic flow), and statistics [11].

In support of better technology, the Physics Research Division and Development of Physics also suggest that one way of achieving better traffic flow is by ACC. They propose that the behavior of traffic flow has origins in phase transitions, hysteresis, and historical dependence. Their article relates the relevance of vehicular density, flux, and synchronized speeds of vehicles as they relate to the behavior of traffic flow. In addition to ACC, the article describes how downstream traffic information can also lead to "jam dissolution". Also, being made aware of information of upcoming vehicles on the road can lead to an alternate driving strategy to avoid a traffic jam that lie ahead [5].

At Shizuoka University in Japan, a group of engineers study the formation of traffic jams with some slowdown sections. In the study they discuss that when slowdown sections of traffic form, they may develop by a single stationary shockwave or by some discontinuous fronts. They go on to discuss that when a saturated flow of traffic occurs, this may be due to the maximal value in the current strongest slowdown sections. Also, they examine how the dependence of traffic jam lengths can be determined numerically and analytically [2].

So, as we can see, there is a considerable interest in understanding the phenomena

Chapter 1. Introduction

of traffic flow. If we can better understand traffic flow, then we may be able to solve more traffic problems, such as traffic jams.

For our model we will be treating the flow of traffic as a continuum having a density defined by the number of cars per unit length. We are considering the simplest case, where the number of cars is conserved, that is, the track for the cars will have no entries or exits. The model involves a numerical simulation leading to a numerical solution of a system of two partial differential equations, one nonlinear, the other, linear. The first is the transport equation of velocity. For the velocity of cars, we are using the general Hopf equation where the right-hand side is a piece-wise function dependent on density and velocity. The second equation is the continuity equation of the density of cars on a closed track. The solution of the system is used to achieve an efficient movement of traffic and minimal traffic congestion. We will be using Matlab for our simulation and solution.

Chapter 2

System of Equations

In this chapter we will be introducing both the transport and continuity equations, and the system of these equations. Then we will explain how we will be modeling the right-hand side of our transport equation. We will be considering the simplest case in the flow of traffic of cars, in that our system of equations is based on the velocity and density of cars traveling in the same direction on a closed, circular track. We consider the flow of traffic as a hydrodynamic model, in that cars traveling on a road behave similarly to the properties of the flow of a fluid. Our model will be similar to the Payne-Whitham model of traffic flow [10]. Our system will consist of a nonlinear inhomogeneous transport equation and a linear homogeneous continuity equation. For this chapter we will be introducing both equations, how we solve the system of equations and how we model the general function of the transport equation that concerns the behavior of the driver. Because cars are all traveling in the same direction on a closed, circular track, the number of cars is conserved. Please note, that although we are considering a simple version of a roadway, we could make adjustments to our model and system of equations to account for the entries and exits to our roadway. We are truly interested in the general results of situations on the roadway that occur due to the various interplays between velocity and density

on a closed track, which we will model.

2.1 Introducing the Transport Equation

For velocity, we consider the Hopf (nonlinear transport or advection) equation

$$u_t + uu_x = f \tag{2.1}$$

where in our case, the right-hand side is a function attempting to model the behavior of the driver. This function will be dependent on both density and velocity. The transport equation is inhomogeneous. The transport equation that we will be using is as follows:

$$v_t + vv_x = f(\rho, v) \tag{2.2}$$

where v is the velocity of cars and ρ is the density of cars, i.e., the number of cars per unit length.

2.2 Introducing the Continuity Equation

The next equation of the system we will be solving is the continuity equation. This is a linear, homogeneous, partial differential equation. Below is the continuity equation that will be used in our system of equations:

$$\rho_t + (\rho v)_x = 0. \tag{2.3}$$

The right-hand side of the continuity equation is zero due to modeling a closed track, without any entrances or exits. By adding a nonzero right-hand side, we can model ramps and exits. But for now, we shall consider the simplest case.

2.3 Solving the System of Equations

After building the arrays for the transport and continuity equations, we will use them in our schemes for solving the system of equations numerically. As a result, we have a system of two partial differential equations which we will solve. This model is what we will use for the system of traffic flow on a circular track. Using a circular track, implies use of periodic boundary conditions. To find an analytical solution of the system is a complex problem. So, through our investigation of this system, we will solve the system numerically, through numerical simulation.

$$\begin{cases} v_t + vv_x & = f(\rho, v) \\ \rho_t + (\rho v)_x & = 0 \end{cases}$$

2.4 Modeling the Right-Hand Side of the Transport Equation

In this section we explain the right-hand side of the transport equation, f , the parameters to be used in our equations, and desired velocity. Some of the parameters will be used to model the desired velocity, v_0 , and the right-hand side of the transport equation, f , as well as its time derivative, f_t . Let us begin by our explanation of parameters to be used in our system of equations.

We want the right-hand side of the transport equation, f , to model the behavior of

Chapter 2. System of Equations

the driver. We build this piece-wise function by the desired velocity v_0 , the maximum velocity at a specific time, v_{max} , and the characteristic time, T_c . The desired velocity, v_0 , will use the density of cars, ρ , and the parameters of the current speed limit, v_{max} , average length of a car, L , and safe-time separation between cars, t_{sep} . The values of these parameters and the building of the desired velocity function will be discussed shortly.

The function will be built as follows:

$$v_0(x, t) = \frac{\rho^{-1}(x, t) - L}{t_{sep}}, \quad (2.4)$$

$$f(\rho, v) = \begin{cases} \frac{v_0 - v}{T_c} & \text{if } v_0 < v_{max} \\ \frac{v_{max} - v}{T_c} & \text{if } v_0 \geq v_{max}. \end{cases} \quad (2.5)$$

After this, we have f_t , the partial derivative of f with respect to time, t , to calculate. Using the power-rule inside the function v_0 , we have:

$$f_t = \begin{cases} -\frac{1}{T_c t_{sep}} \left(\frac{\rho_t}{\rho^2} + t_{sep} v_t \right) & \text{if } v_0 < v_{max} \\ -\frac{1}{T_c} v_t & \text{if } v_0 \geq v_{max} \end{cases} \quad (2.6)$$

2.4.1 Parameters

For our first constant, we consider the length of our circular track to be 10 miles. We set the number of grid steps at $N = 10,000$. We are using the average length of a car, L , as being equal to five yards (or fifteen feet). For our numerical scheme, the grid step size, h , will be the length of our track divided by the number of grids steps, yielding $h = 0.001$.

Chapter 2. System of Equations

Let T_c be the characteristic time, $v(t, x)$ be velocity of a car on the track as a function of time t and x , and v_i be the initial velocity (at time $t = 0$ seconds). Our model corresponds to exponential change of v , so we can say that

$$v(t) = v_i e^{\frac{t}{T_c}}. \quad (2.7)$$

Let us suppose that we want to change our velocity from 60mph to 75mph. For a typical car it takes approximately 3 seconds to do this. And so, we have the following equation for T_c :

$$75 = 60e^{\frac{3}{T_c}} \quad \Rightarrow \quad (2.8)$$

$$\ln \frac{5}{4} = \frac{3}{T_c} \quad \Rightarrow \quad (2.9)$$

$$T_c = \frac{3}{\ln 1.25} \quad (2.10)$$

$$\approx 13.4443 \text{ sec} \quad (2.11)$$

$$= 0.003735 \text{ hours.} \quad (2.12)$$

Next, let t_{sep} be the safe-time separation between cars. Then, by the driver's manual by DMV, New Mexico, we have the safe-time separation of $t_{sep} = 2 \text{ sec} = 0.000\bar{5} \text{ hours}$ [6].

2.4.2 Desired Velocity

What follows is our explanation of desired (or “safe”) velocity v_0 . We are treating the right-hand side of the transport equation as a general function dependent on density and velocity. This is done by our interpretation of a driver's desired velocity, v_0 . We will see how the right-hand side of the transport equation is derived in the next chapter. For now we will examine how our desired velocity, v_0 is derived.

Cars are trying to reach their desired velocity. This desired velocity cannot be higher than the maximum velocity of the road (speed limit). And so, if a driver is

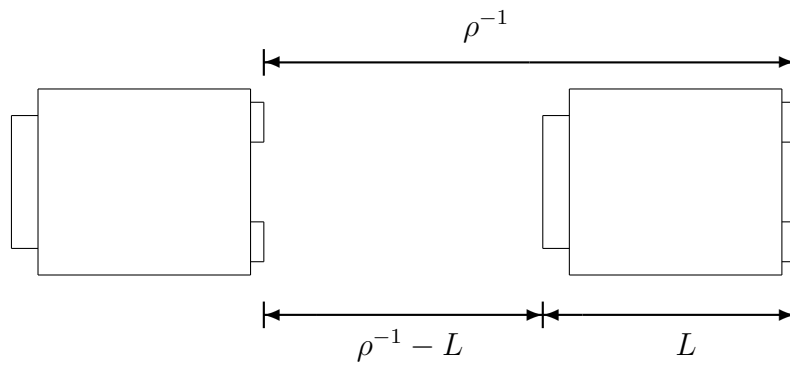
Chapter 2. System of Equations

traveling faster than the speed limit, then the desired velocity is to return to the speed limit. On the other hand, if the driver is traveling slower than the speed limit, then the desired velocity is to increase toward the speed limit. In this case, density needs to be taken into consideration. So, velocity changes based upon the current density, the speed limit, the current velocity, and the desired velocity. We also see how this change depends upon how our desired velocity v_0 compares to the speed limit v_{max} . On the road, the speed limit becomes a crucial aspect of how we view the driver's desired velocity v_0 . If $v < \min\{v_0, v_{max}\}$, the driver desires to speed-up in order to try and attain the desired speed. On the other hand, if the driver is speeding, then the driver will want to slow-down.

Also related to the driver's desired velocity v_0 , are the conditions for each piece of the function for v_0 . If $\rho \neq 0$ (where ρ is density of the cars), then the driver is not alone on the road. On the other hand, the other situation is where the driver is alone and we consider the density, ρ , equal to zero. For the value of the function for desired velocity, v_0 , when density is zero, it is the maximum velocity. When density is other than zero, our desired velocity relates to other cars on the road. For this desired velocity, it is the distance between cars divided by the safe-time separation (the safe-time separation is taken to be a constant of 2 seconds as stated above). The distance between cars is taken to be the difference between the reciprocal of the current value of density less the average length of a car, L , equal to five yards.

The interpretation of the distance between cars is to begin with the reciprocal of the density of our cars on the track. The reciprocal of density is taken to be the length of an average car plus the distance between that car's rear bumper and the front bumper of another car behind it. So, to subtract the average length of a car from the reciprocal of density is the "distance" between cars. Then, dividing this distance by the safe-time separation, we get our desired velocity when other cars are on the road.

Figure 2.1: Distance between cars



Chapter 3

Numerical Scheme

In this chapter we will be deriving our numerical schemes, evaluating the stability conditions for each scheme, and also investigating the error approximations of each scheme. For the sections on error approximation, we will need to verify that our simulations are second order in both time and space. We will show this through charts and tables that show our errors vary quadratically in both time and space with the change of time and coordinate steps.

One condition for solving both equations is a choice for the time-step, which we will call τ . For the maximum velocity $\max |v|$, at each grid spacing h , we use the Courant-Friedrich-Lewy condition for our choice of τ , i.e. $\tau \leq a \frac{h}{\max |v|}$, for $0 \leq a < 1$. For our simulations we used $a = 0.1$ (see sections 3.3 and 3.6 on error approximation)[8]. When describing how our errors vary in this chapter, we will refer to this specific number a as our “CFL factor”.

3.1 Numerical Scheme for the Transport Equation

As will be seen in this chapter for our numerical schemes, in order to get second order in both time and space, we will use the Taylor expansion for both equations up through the third term.

This leads us to the numerical scheme for the transport equation. Since the transport equation is inhomogeneous, we need to handle our non-zero right-hand side of the equation, f , differently from the “zero” right-hand side of the equation for the continuity equation. Because we are considering the transport of the velocity field by itself, we first want to derive the scheme for the transport equation.

We begin with the basic transport equation

$$v_t + vv_x = f \tag{3.1}$$

and solve for the partial derivative of v with respect to t , namely,

$$v_t = f - vv_x \tag{3.2}$$

$$= f - \frac{1}{2} \cdot \frac{\partial}{\partial x}(v^2). \tag{3.3}$$

We use (3.3) to substitute later in our scheme. Then, using

$$\left. \frac{\partial f}{\partial x} \right|_{x=x_j} = \underbrace{\frac{f_{j+1} - f_{j-1}}{2h}}_{\text{2nd order scheme}} \tag{3.4}$$

Chapter 3. Numerical Scheme

and the Taylor expansion of $v(t + \tau)$, we have

$$v(t + \tau) \approx v(t) + v_t \tau + \frac{1}{2} \cdot \frac{\partial}{\partial t}(v_t) \tau^2 \quad (3.5)$$

$$= v(t) + v_t \tau + \frac{1}{2} \cdot \frac{\partial}{\partial t} \left[f - \frac{1}{2} \frac{\partial}{\partial x}(v^2) \right] \tau^2 \quad (3.6)$$

$$= v(t) + v_t \tau + \frac{\tau^2}{2} \left[f_t - \frac{1}{2} \frac{\partial}{\partial t} \frac{\partial}{\partial x}(v^2) \right] \quad (3.7)$$

$$= v(t) + v_t \tau + \frac{\tau^2}{2} \left[f_t - \frac{1}{2} \frac{\partial}{\partial x} \frac{\partial}{\partial t}(v^2) \right] \quad (3.8)$$

$$= v(t) + v_t \tau + \frac{\tau^2}{2} \left[f_t - \frac{1}{2} \frac{\partial}{\partial x}(2vv_t) \right] \quad (3.9)$$

$$= v(t) + v_t \tau + \frac{\tau^2}{2} \left[f_t - \frac{\partial}{\partial x}(vv_t) \right]. \quad (3.10)$$

From what was written above, this directly translates into our code for finding the next value of time for velocity, thereby solving the transport equation:

$$v_1^{n+1} = v_1^n + (v_t)_1^n \tau + \frac{\tau^2}{2} \left\{ (f_t)_1^n - \frac{1}{2h} [(vv_t)_2^n - (vv_t)_N^n] \right\}, \quad (3.11)$$

$$v_j^{n+1} = v_j^n + (v_t)_j^n \tau + \frac{\tau^2}{2} \left\{ (f_t)_j^n - \frac{1}{2h} [(vv_t)_{j+1}^n - (vv_t)_{j-1}^n] \right\}, \text{ for } j = 2, \dots, N-1 \quad (3.12)$$

$$v_N^{n+1} = v_N^n + (v_t)_N^n \tau + \frac{\tau^2}{2} \left\{ (f_t)_N^n - \frac{1}{2h} [(vv_t)_1^n - (vv_t)_{N-1}^n] \right\}. \quad (3.13)$$

Now, this leads us to building certain arrays to be used in our numerical scheme in order to find the next value of time for the transport equation. This value will estimate our derivative for velocity v with respect to time.

The next four arrays that need to be built will be for the transport equation. First, we have $(v_t)_j^n$ which uses f_j^n , which can be seen being built below:

$$(v_t)_1^n = f_1^n - \frac{1}{4h} [(v_2^n)^2 - (v_N^n)^2], \quad (3.14)$$

Chapter 3. Numerical Scheme

$$(v_t)_j^n = f_j^n - \frac{1}{4h}[(v_{j+1}^n)^2 - (v_{j-1}^n)^2], \text{ for } j = 2, \dots, N - 1 \quad (3.15)$$

$$(v_t)_N^n = f_N^n - \frac{1}{4h}[(v_1^n)^2 - (v_{N-1}^n)^2]. \quad (3.16)$$

Next, we introduce $(vv_t)_j^n = (v_j^n)(v_t)_j^n$ which we get in our code again by term-wise products of arrays:

$$vv_t = v \cdot v_t. \quad (3.17)$$

Translating our right-hand side of the transport equation numerically, we have:

$$f_j^n = \begin{cases} \frac{1}{T_c}[(v_0)_j^n - v_j^n] & \text{if } (v_0)_j^n < (v_{max})_j \\ \frac{1}{T_c}[(v_{max})_j^n - v_j^n] & \text{if } (v_0)_j^n \geq (v_{max})_j \end{cases} \quad (3.18)$$

for $j = 1, \dots, N$.

The last array to build is f_t . This will also be used to find the next value of time for velocity. And so, for our code we have:

$$(f_t)_j^n = \begin{cases} -\frac{1}{T_c t_{sep}} \left[\frac{(\rho_t)_j^n}{(\rho_j^n)^2} + t_{sep}(v_t)_j^n \right] & \text{if } (v_0)_j^n < (v_{max})_j \\ -\frac{1}{T_c}(v_t)_j^n & \text{if } (v_0)_j^n \geq (v_{max})_j \end{cases} \quad (3.19)$$

for $j = 1, \dots, N$.

After building these arrays, we will use them in our scheme for solving the transport equation.

This leads us to how we find the next value of time for velocity. In the next section, we investigate the stability conditions for the transport equation.

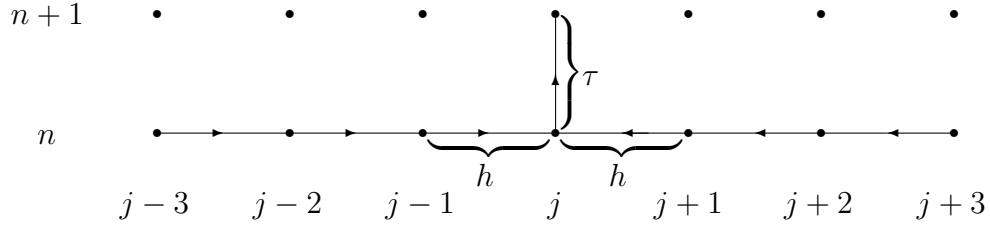
3.2 Stability Conditions for the Transport Equation

Let us consider a nonlinear transport equation:

$$u_t + uu_x = 0 \quad t > 0, -\infty < x < \infty \quad (3.20)$$

$$u(x, 0) = \phi(x) \quad (3.21)$$

Figure 3.1: Schematic representation of our numerical scheme



In order to analyze stability, we cannot use $u_j^n = \xi^n e^{ikjh}$ because it is not a solution to a nonlinear equation. Solving for u_j^{n+1} we have:

$$u_j^{n+1} = u_j^n + \tau \left[f_j^n - \frac{1}{2} \frac{(u_{j+1}^n)^2 - (u_{j-1}^n)^2}{2h} \right] + \frac{\tau^2}{2} \left[g_j^n - \frac{u_{j+1}^n f_{j+1}^n - u_{j-1}^n f_{j-1}^n}{2h} + \frac{1}{3} \frac{(u_{j+1}^n)^3 - 2(u_j^n)^3 + (u_{j-1}^n)^3}{h^2} \right] \quad (3.22)$$

Let us notice that the second derivative has to be finite. Now, if we let $f = g = 0$ and $u_j^n = \bar{u}_j^n + \delta_j^n$ for the exact solution, \bar{u}_j^n and the error δ_j^n then, by substitution

Chapter 3. Numerical Scheme

(leaving only linear terms in δ), we have:

$$\delta_j^{n+1} = \delta_j^n - \frac{\tau}{4h} (2u_{j+1}^n \delta_{j+1} - u_{j-1}^n \delta_{j-1}) \quad (3.23)$$

$$\begin{aligned} & + \frac{\tau^2}{2 \cdot 3h^2} [3(u_{j+1}^n)^2 \delta_{j+1}^n - 2 \cdot 3(u_j^n)^2 \delta_j^n \\ & + 3(u_j^n)^2 \delta_j^n + 3(u_{j-1}^n)^2 \delta_j^n + 3(u_{j-1}^n)^2 \delta_{j-1}^n] \\ & = \delta_j^n - \frac{\tau^2}{2h} (u_{j+1}^n \delta_{j+1}^n - u_{j-1}^n \delta_{j-1}^n) \quad (3.24) \\ & + \frac{\tau^2}{2h^2} [(u_{j+1}^n)^2 \delta_{j+1}^n - 2(u_j^n)^2 \delta_j^n + (u_{j-1}^n)^2 \delta_{j-1}^n] \end{aligned}$$

Then, if we let $\delta_j^n = C \lambda^n e^{ikjh}$ and solve for λ , we have:

$$\begin{aligned} \lambda & = 1 - \frac{\tau}{2h} (u_{j+1}^n e^{ikh} - u_{j-1}^n e^{-ikh}) \quad (3.25) \\ & + \frac{\tau^2}{2h^2} [(u_{j+1}^n)^2 e^{ikh} - 2(u_j^n)^2 + (u_{j-1}^n)^2 e^{-ikh}] \end{aligned}$$

Let us try to estimate λ . If we use the von Neumann stability criterion [3], then, $|\lambda| \leq 1 + |c_1| \tau$, for some finite constant c_1 . Now, let us use the method of “frozen coefficients [7],” where we let $\rho = \frac{\tau}{h} u_j^n$. Then, after some bulky calculations (and letting $\alpha = kh$), we get:

$$1 - 4\rho^2 \sin^4 \frac{\alpha}{2} + 4\rho^4 \sin^4 \frac{\alpha}{2} \leq 1. \quad (3.26)$$

After solving for ρ , we get $\rho^2 \leq 1$.

Then, this implies:

$$\left| \frac{\tau}{h} u_j^n \right| \leq 1 \quad (3.27)$$

and the von Neumann stability criterion is satisfied.

There is an additional condition for stability, that $\left| \frac{\partial u}{\partial x} \right| \leq c_2$, for some constant $c_2 < \infty$. This in turn, implies a finite $\left| \frac{\partial u}{\partial x} \right|$.

Also, notice that the limitation for $\tau = t_{n+1} - t_n \leq \frac{h}{\max_{j,n} \|u_j^n\|}$.

3.3 Error Approximation for the Transport Equation

To show that our errors vary quadratically with respect to time, we set our number of time-steps to 10,000, use a CFL-factor of 0.1 and set the number of grid steps to 1000 for our “general” case. The final time of simulation was 1.0 hours. Then we compare results for having a specific number time steps to the results for our reference case where there were 10,000 time steps. The parameters were a track length of 2π miles, 3 cycles, for a total period of 6π miles. In order to find the accuracy of our numerical scheme for the transport equation

$$v_t + vv_x = f(\rho, v), \tag{3.28}$$

we used the initial condition of

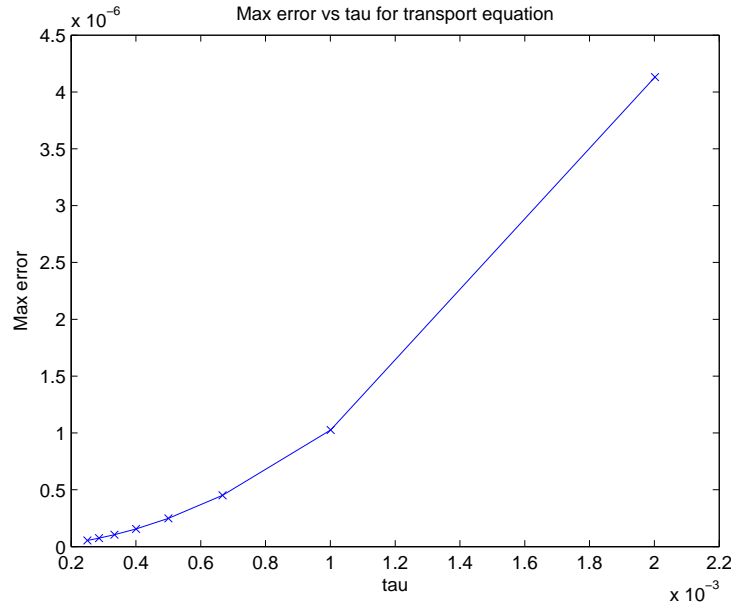
$$v(x, 0) = \sin(A_0x) \tag{3.29}$$

and the right-hand side of

$$f(x, t) = -\sin t \cdot \sin(A_0x) + \cos^2 t \cdot \sin(A_0x) \cdot \cos(A_0x) \tag{3.30}$$

(fabricated solution), where the parameter $A_0 = 6\pi \cdot 10^{-3}$, to yield the computed solution. The initial condition and right-hand side were chosen so that the exact solution could be found by hand. As seen in the charts and tables, the number of time steps will take on the values of N . The different number of time steps comparing to the reference case will have the values of: 500, 1000, 1500, 2000, 2500, 3000, 3500, and 4000. For the varying number of time steps, we used a CFL-factor of 0.1 and set the number of grid steps to 1000. As can be seen from the chart and table, our errors with respect to time for the numerical scheme of the transport equation, vary quadratically. We also include a log vs log graph to see linearly that our errors truly are varying quadratically with respect to time.

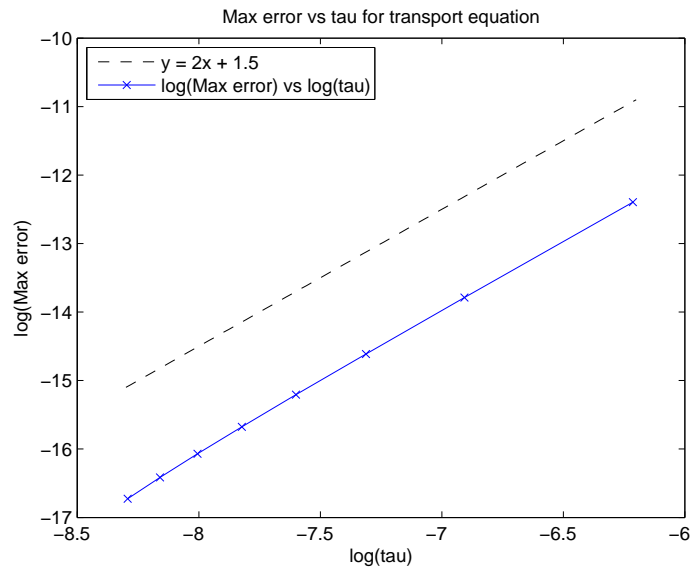
Figure 3.2: Transport: Max Error vs. τ



Then, to show our errors vary quadratically with respect to the space step (in our case, space is the one-dimensional x -space step), we use the exact (fabricated) solution to a specific number of grid steps. We compare the exact solution

$$u(x, t) = \cos t \cdot \sin(A_0 x) \tag{3.31}$$

to the computed solution. We used a CFL factor of 0.1. For the number of grid steps that vary, they will take on the same values that were used for the varying number of time steps in the previous section, namely: 500, 1000, 1500, 2000, 2500, 3000, 3500, and 4000. As can be seen from the chart and table, our errors with respect to space for the numerical scheme of the transport equation, vary quadratically. Again, we include a log vs log graph to view linearly that our errors truly are varying quadratically, in this case, with respect to space.

Figure 3.3: Transport: $\log(\text{Max Error})$ vs. $\log(\tau)$ 

3.4 Numerical Scheme for the Continuity Equation

In order to solve the continuity equation numerically, we begin by building the array for $(\rho_t)_j^n$. Instead of building this array from inception, we first build the array $\rho v_x = \rho_j^n \cdot (v_x)_j^n$ and use the fact that from the continuity equation, $\rho_t = -\rho v_x$ to derive in our code that $(\rho_t)_j^n = -\rho_j^n \cdot (v_x)_j^n$. The next array is also built by multiplying arrays “term-wise”, namely, $(\rho_t v)_j^n = (\rho_t)_j^n \cdot v_j^n$. Lastly, we again build the next array by term-wise multiplication of arrays, namely, $(\rho v_t)_j^n = \rho_j^n \cdot (v_t)_j^n$. This uses v_t which can be seen being built above in the arrays for the transport equation.

Using the arrays we just built, these will be used in the scheme below for the continuity equation (and again, uses the schematic representation seen in Figure 3.1). What follows is our method for solving the continuity equation. Starting from

Chapter 3. Numerical Scheme

Table 3.1: Transport Equation Errors, τ vs. N

τ	N	Max Error with respect to “exact” solution
0.0020018228	500	0.00000413162802
0.0010009114	1000	0.00000102659930
0.0006672743	1500	0.00000045071714
0.0005004557	2000	0.00000024904742
0.0004003646	2500	0.00000015567609
0.0003336371	3000	0.00000010494673
0.0002859747	3500	0.00000007435476
0.0002502279	4000	0.00000005449762

Table 3.2: Transport Equation Errors, h vs. N

h	N	Max Error with respect to exact solution
0.0376991118	500	0.00047137127720
0.0188495559	1000	0.00011782132857
0.0125663706	1500	0.00005239861284
0.009424778	2000	0.00002948261787
0.0075398224	2500	0.00001886185223
0.0062831853	3000	0.00001309512870
0.0053855874	3500	0.00000962290281
0.004712389	4000	0.00000736863092

$\rho_t + \frac{\partial}{\partial x}(\rho v) = 0$ and solving for ρ_t , $\rho_t = -\frac{\partial}{\partial x}(\rho v)$. Then, using

$$\left. \frac{\partial f}{\partial x} \right|_{x=x_j} = \underbrace{\frac{f_{j+1} - f_{j-1}}{2h}}_{\text{2nd order scheme}} \quad (3.32)$$

and the Taylor expansion of $\rho(t + \tau)$, and replacement of our partial derivative, ρ_t , we have

$$\rho(t + \tau) \approx \rho(t) + \frac{\partial \rho}{\partial t} \tau + \frac{1}{2} \cdot \frac{\partial^2 \rho}{\partial t^2} \tau^2 \quad (3.33)$$

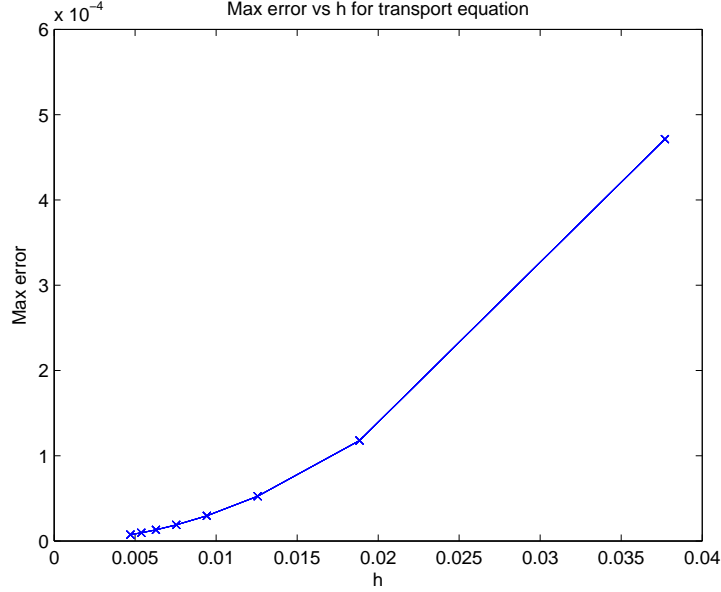
$$= \rho(t) - \frac{\partial}{\partial x}(\rho v) \tau + \frac{1}{2} \cdot \frac{\partial}{\partial t} \left[-\frac{\partial}{\partial x}(\rho v) \right] \tau^2 \quad (3.34)$$

$$= \rho(t) - \frac{\partial}{\partial x}(\rho v) \tau + \frac{1}{2} \cdot \frac{\partial}{\partial x} \left[-\frac{\partial}{\partial t}(\rho v) \right] \tau^2 \quad (3.35)$$

$$= \rho(t) - \frac{\partial}{\partial x}(\rho v) \tau - \frac{\tau^2}{2} \cdot \frac{\partial}{\partial x} \left[-v \frac{\partial}{\partial x}(\rho v) + v_t \rho \right] \quad (3.36)$$

Chapter 3. Numerical Scheme

Figure 3.4: Transport: Max Error vs. h



From what is written above, we now will see what translates to our code for finding the next value for density with respect to time. And so, the next value of density is as follows:

$$\rho_1^{n+1} = \rho_1^n - \frac{\tau}{2h}(\rho_2^n v_2^n - \rho_N^n v_N^n) \quad (3.37)$$

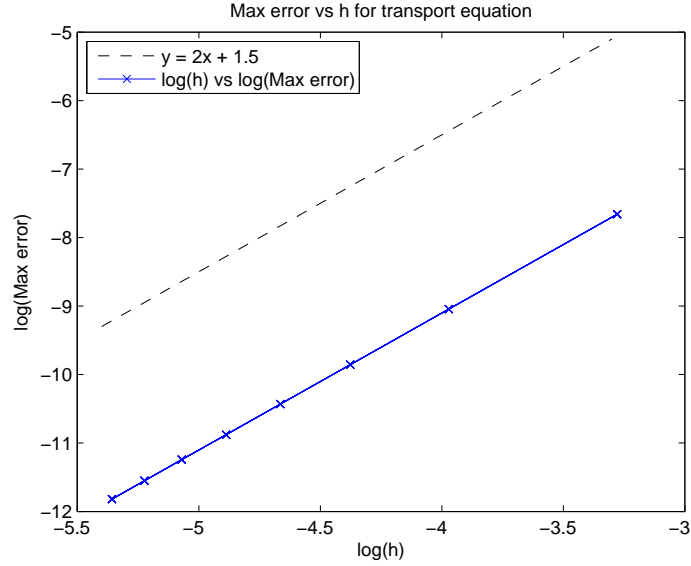
$$- \frac{\tau^2}{2} \frac{\partial}{\partial x} \left[v_1^n \frac{\rho_2^n v_2^n - \rho_N^n v_N^n}{2h} + (v_t)_1^n \rho_1^n \right]$$

$$= \rho_1^n - \frac{\tau}{2h}(\rho_2^n v_2^n - \rho_N^n v_N^n) \quad (3.38)$$

$$+ \frac{\tau^2}{4h} \left[v_2^n \frac{\rho_3^n v_3^n - \rho_1^n v_1^n}{2h} - v_N^n \frac{\rho_1^n v_1^n - \rho_{N-1}^n v_{N-1}^n}{2h} \right.$$

$$\left. - (v_t)_2^n \rho_2^n + (v_t)_N^n \rho_N^n \right], \quad (3.39)$$

Figure 3.5: Transport: $\log(\text{Max Error})$ vs. $\log(h)$



$$\rho_2^{n+1} = \rho_2^n - \frac{\tau}{2h}(\rho_3^n v_3^n - \rho_1^n v_1^n) \quad (3.40)$$

$$- \frac{\tau^2}{2} \frac{\partial}{\partial x} \left[v_2^n \frac{\rho_3^n v_3^n - \rho_1^n v_1^n}{2h} + (v_t)_2^n \rho_2^n \right]$$

$$= \rho_2^n - \frac{\tau}{2h}(\rho_3^n v_3^n - \rho_1^n v_1^n) \quad (3.41)$$

$$+ \frac{\tau^2}{4h} \left[v_3^n \frac{\rho_4^n v_4^n - \rho_2^n v_2^n}{2h} - v_1^n \frac{\rho_2^n v_2^n - \rho_N^n v_N^n}{2h} \right.$$

$$\left. - (v_t)_3^n \rho_3^n + (v_t)_1^n \rho_1^n \right], \quad (3.42)$$

Chapter 3. Numerical Scheme

$$\rho_j^{n+1} = \rho_j^n - \frac{\tau}{2h}(\rho_{j+1}^n v_{j+1}^n - \rho_{j-1}^n v_{j-1}^n) \quad (3.43)$$

$$- \frac{\tau^2}{2} \frac{\partial}{\partial x} \left[v_j^n \frac{\rho_{j+1}^n v_{j+1}^n - \rho_{j-1}^n v_{j-1}^n}{2h} + (v_t)_j^n \rho_j^n \right]$$

$$= \rho_j^n - \frac{\tau}{2h}(\rho_{j+1}^n v_{j+1}^n - \rho_{j-1}^n v_{j-1}^n) \quad (3.44)$$

$$+ \frac{\tau^2}{4h} \left[v_{j+1}^n \frac{\rho_{j+2}^n v_{j+2}^n - \rho_j^n v_j^n}{2h} - v_{j-1}^n \frac{\rho_j^n v_j^n - \rho_{j-2}^n v_{j-2}^n}{2h} \right.$$

$$\left. - (v_t)_{j+1}^n \rho_{j+1}^n + (v_t)_{j-1}^n \rho_{j-1}^n \right], \text{ for } j = 3, \dots, N-2 \quad (3.45)$$

$$\rho_{N-1}^{n+1} = \rho_{N-1}^n - \frac{\tau}{2h}(\rho_N^n v_N^n - \rho_{N-2}^n v_{N-2}^n) \quad (3.46)$$

$$- \frac{\tau^2}{2} \frac{\partial}{\partial x} \left[v_{N-1}^n \frac{\rho_N^n v_N^n - \rho_{N-2}^n v_{N-2}^n}{2h} + (v_t)_{N-1}^n \rho_{N-1}^n \right]$$

$$= \rho_{N-1}^n - \frac{\tau}{2h}(\rho_N^n v_N^n - \rho_{N-2}^n v_{N-2}^n) \quad (3.47)$$

$$+ \frac{\tau^2}{4h} \left[v_N^n \frac{\rho_1^n v_1^n - \rho_{N-1}^n v_{N-1}^n}{2h} - v_{N-2}^n \frac{\rho_{N-1}^n v_{N-1}^n - \rho_{N-3}^n v_{N-3}^n}{2h} \right.$$

$$\left. - (v_t)_N^n \rho_N^n + (v_t)_{N-2}^n \rho_{N-2}^n \right], \quad (3.48)$$

$$\rho_N^{n+1} = \rho_N^n - \frac{\tau}{2h}(\rho_1^n v_1^n - \rho_{N-1}^n v_{N-1}^n) \quad (3.49)$$

$$- \frac{\tau^2}{2} \frac{\partial}{\partial x} \left[v_N^n \frac{\rho_1^n v_1^n - \rho_{N-1}^n v_{N-1}^n}{2h} + (v_t)_N^n \rho_N^n \right]$$

$$= \rho_N^n - \frac{\tau}{2h}(\rho_1^n v_1^n - \rho_{N-1}^n v_{N-1}^n) \quad (3.50)$$

$$+ \frac{\tau^2}{4h} \left[v_1^n \frac{\rho_2^n v_2^n - \rho_N^n v_N^n}{2h} - v_{N-1}^n \frac{\rho_N^n v_N^n - \rho_{N-2}^n v_{N-2}^n}{2h} \right.$$

$$\left. - (v_t)_1^n \rho_1^n + (v_t)_{N-1}^n \rho_{N-1}^n \right]. \quad (3.51)$$

3.5 Stability Conditions for the Continuity Equation

Then, if we continue with the stability analysis, by letting $\rho_j^n = c_3 \xi^n e^{ikh}$ and $v_{j+1}^n = v_j^n + \frac{\partial v}{\partial x} h$, after substitution and some calculations we will get:

$$\begin{aligned} \xi = 1 - \frac{\tau}{2h} \left[i v_j^n \sin(kh) + \frac{\partial v}{\partial x} h \cos(kh) \right] \\ + \frac{\tau^2}{2h} \left[-\frac{(v_j^n)^2}{h} \sin^2(kh) + i \frac{3}{2} \frac{\partial v}{\partial x} v_j^n \sin(2kh) + \left(\frac{\partial v}{\partial x} \right)^2 h \cos(2kh) \right. \\ \left. - i (v_t)_j^n \sin(kh) - v_{tx} h \cos(kh) \right]. \end{aligned} \quad (3.52)$$

Then, by using “frozen coefficients”, if we let $\epsilon = \frac{\tau v_j^n}{h} \sin(kh)$, $b = \frac{\partial v}{\partial x} \cos(kh)$, and $a = \frac{(v_t)_j^n}{v_j^n}$, then we will get

$$\xi = 1 - \frac{1}{2} b \tau - \frac{1}{2} \epsilon^2 - i \frac{\epsilon}{2} (1 - 2b\tau + a\tau). \quad (3.53)$$

Using this to continue to verify stability conditions we have:

$$|\xi|^2 = \left(1 - \frac{1}{2} b \tau - \frac{1}{2} \epsilon^2 \right)^2 + \frac{\epsilon^2}{2} (1 - 3b\tau + a\tau)^2 \quad (3.54)$$

$$\begin{aligned} = \left(1 - \frac{1}{2} b \tau \right)^2 - \left(1 - \frac{1}{2} b \tau \right) \epsilon^2 + \frac{1}{4} \epsilon^4 \\ + \frac{\epsilon^2}{2} [(1 - 3b\tau)^2 + 2a\tau(1 - 3b\tau) + a^2\tau^2]. \end{aligned} \quad (3.55)$$

By omitting terms with τ^2 and higher powers we have:

$$|\xi|^2 = 1 - b\tau - \epsilon^2 + \frac{1}{2} b\tau\epsilon^2 + \frac{1}{4}\epsilon^4 + \frac{\epsilon^2}{2} - 3\epsilon^2 b\tau + a\tau\epsilon^2 \quad (3.56)$$

$$= 1 - \frac{1}{2}\epsilon^2 + \frac{1}{4}\epsilon^4 + \left(\frac{1}{2} b\epsilon^2 - 3\epsilon^2 b + a\epsilon^2 \right) \tau \quad (3.57)$$

$$= 1 - \frac{1}{2}\epsilon^2 + \frac{1}{4}\epsilon^4 + \left(-\frac{5}{2}b + a \right) \epsilon^2 \tau. \quad (3.58)$$

Chapter 3. Numerical Scheme

If we let $(-\frac{5}{2}b + a) = c_4$ for $|c_4| < \infty$, then for $1 - \frac{1}{2}\epsilon^2 + \frac{1}{4}\epsilon^4 \leq 1$ we have:

$$|\xi|^2 = 1 - \frac{1}{2}\epsilon^2 + \frac{1}{4}\epsilon^4 + c_4\epsilon^2\tau \quad (3.59)$$

$$\leq 1 + c_4\epsilon^2\tau \quad (3.60)$$

and the von Neumann stability criterion has been satisfied. With this, if we continue solving for ϵ , we have :

$$\frac{1}{2}\epsilon^2 \left(\epsilon^2 - \frac{1}{2} \right) \leq 0. \quad (3.61)$$

This implies:

$$\epsilon^2 \leq \frac{1}{2} \quad \text{and} \quad |\epsilon| \leq \frac{1}{\sqrt{2}}. \quad (3.62)$$

So, in turn, this implies that we will have one condition for stability for

$$\tau \leq \frac{1}{\sqrt{2}} \frac{h}{\max_{j,n} v_j^n} \quad (3.63)$$

which implies

$$\tau < 0.7 \frac{h}{\max_{j,n} v_j^n}. \quad (3.64)$$

Overall, we will have stability for τ being less than the CFL factor of 0.7 (for our simulations we will be using the CFL factor of 0.1 to ensure stability).

Another condition is that b and a both have to be finite in order for c_4 to be finite. Our final condition for stability is that $|\frac{\partial v}{\partial x}|$ and $|\frac{v_t}{v}|$ both have to be finite. This requires that v_t is finite and $v \neq 0$. Together, these three conditions verify that we have satisfied stability conditions for our numerical scheme for the continuity equation.

3.6 Error Approximation for the Continuity Equation

To show that our errors vary quadratically with respect to time, we used exactly the same method for the continuity equation as we did for the transport equation, i.e., we used the result of the computed solution with the number of time steps set at 10,000 as a reference case over the time interval $[0, 1]$. The varying number of time steps used to compare with the reference case are the same as listed above for the transport equation. The same parameters were used for the error approximation of the continuity equation as were used for the transport equation. In order to find the accuracy of our numerical scheme for the continuity equation

$$\rho_t + (\rho v)_x = 0, \tag{3.65}$$

we used the initial conditions of

$$v(x, 0) = 1 \tag{3.66}$$

and

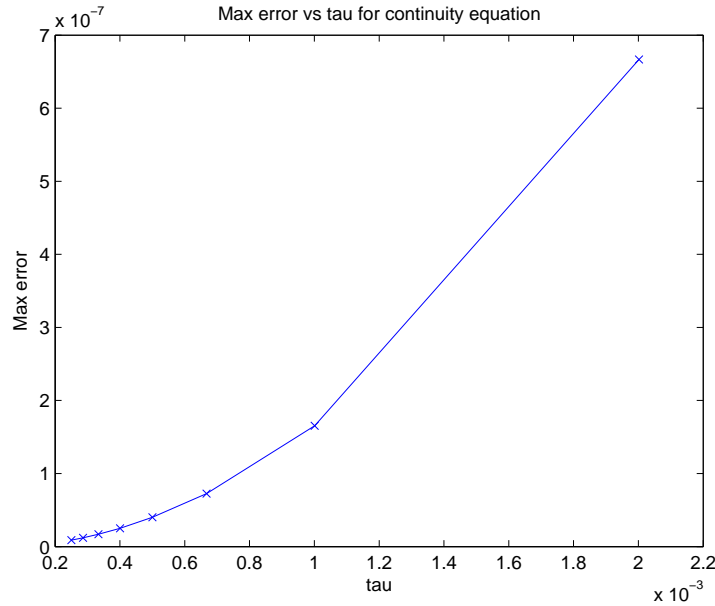
$$\rho(x, 0) = \sin(A_0 x) \tag{3.67}$$

(with a right-hand side of 0), to yield the computed solution. As can be seen from the chart and table, our errors with respect to time for the numerical scheme of the transport equation, vary quadratically. We also include a log vs log graph for errors in the continuity equation with respect to time.

Next, to show our errors vary quadratically with respect to space (again, our space is the one-dimensional x -space), we use the exact solution to a specific number of grid steps. The exact (fabricated) solution was

$$\rho(x, t) = \sin[A_0 x - v(x, 0) \cdot t] \tag{3.68}$$

Figure 3.6: Continuity: Max Error vs. τ



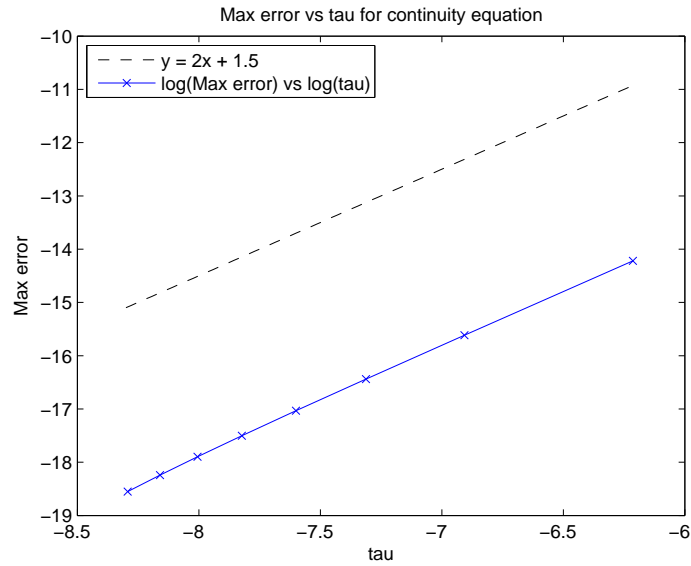
The initial conditions were as before, but the number of spacial grid steps was changing. These number of grid steps vary, and again, take on the same values that were used for showing the varying number of time steps. As can be seen from the chart and table, our errors with respect to space for the numerical scheme of the continuity equation, vary quadratically. Lastly, again, we include a log vs log graph for errors in the continuity equation with respect to space.

We have just shown that our errors vary quadratically with respect to time and space for both the transport and continuity equations. This implies that the numerical scheme for our system of equations is second order for both time and space.

Let us suppose that the length of the track is 10 miles. Then, if the number of grid points is 10,000, each car covers three grid-points, since we consider the average length of our car to be 5 yards (15 feet). Also, since we are not interested in individual cars, rather the behavior of the cars in general, we consider the results of velocity in terms of a “point-average”. This means that instead of each individual point on the

Chapter 3. Numerical Scheme

Figure 3.7: Continuity: $\log(\text{Max Error})$ vs. $\log(\tau)$



grid representing the velocity of only that point, each point of velocity is an average of two points ahead, two points behind, and the three points that each car covers (for an average of seven points). This is a way to more accurately view the velocity and behavior of velocity in our model. Also, as we saw in the previous section, it allows us to satisfy stability conditions, namely, finiteness of the derivative of velocity.

Chapter 3. Numerical Scheme

Table 3.3: Continuity Equation Errors, τ vs. N

τ	N	Max Error with respect to “exact” solution
0.0020018228	500	0.00000066670140
0.0010009114	1000	0.00000016542207
0.0006672743	1500	0.00000007259261
0.0005004557	2000	0.00000004010230
0.0004003646	2500	0.00000002506393
0.0003336371	3000	0.00000001689495
0.0002859747	3500	0.00000001196930
0.0002502279	4000	0.00000000877237

Table 3.4: Continuity Equation Errors, h vs. N

h	N	Max Error with respect to exact solution
0.0376991118	500	0.00023514157845
0.0188495559	1000	0.00005867783290
0.0125663706	1500	0.00002609550171
0.009424778	2000	0.00001468347395
0.0075398224	2500	0.00000939212838
0.0062831853	3000	0.00000651985258
0.0053855874	3500	0.00000479139453
0.004712389	4000	0.00000366915198

Figure 3.8: Continuity: Max Error vs. h

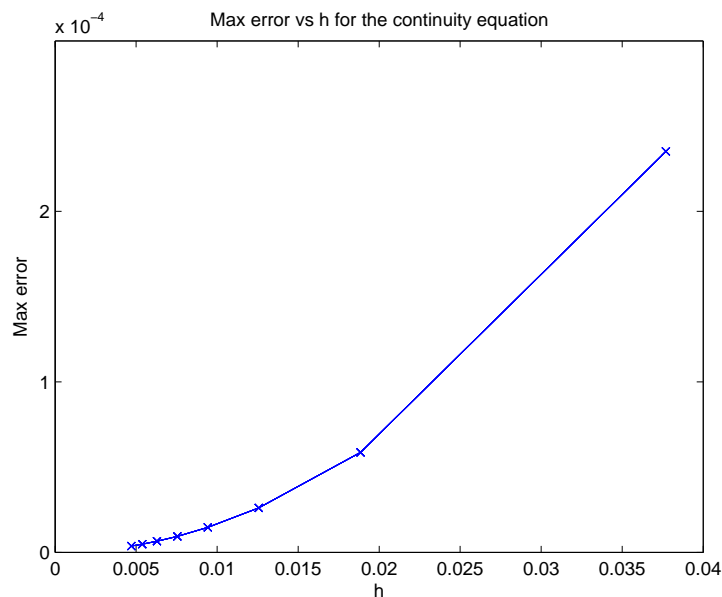
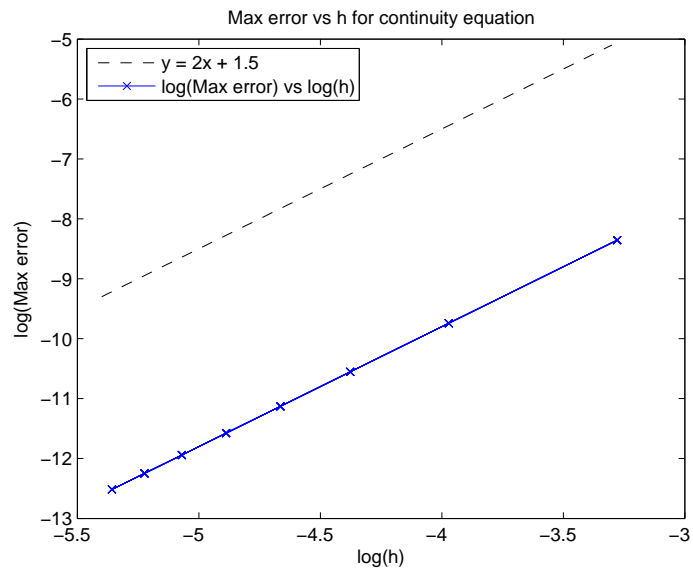


Figure 3.9: Continuity: $\log(\text{Max Error})$ vs. $\log(h)$



Chapter 4

Modeling

This section is to describe the scenarios of road conditions. Certain road conditions directly relate to how the speed limit, v_{max} , is changed. The speed limit had two basic settings: 75mph and 25mph. For the five different scenarios that were simulated, velocity started at 75mph, went down to 25mph, and then returned to 75mph. Within the scenarios, we used a “smoothing” function that helped simulate an abrupt or smooth change in speed limit. The smoothing function used was the inverse tangent function.

Another aspect of our scenarios was the density of cars. For four of the scenarios, we simulated a high density of cars. Then, we considered density either to be homogeneous, that is, “spread-out” or “flat”; or inhomogeneous, as in a “tightly-packed” concentration of cars in an otherwise fairly empty road.

In order to achieve the different types of densities considered above for our scenarios we used two types of density variables. In order for cars to drive at the speed of 75mph on our 10 mile track, we found that our maximum capacity was approximately 22.3 cars per mile. So setting a lower density limit for the cars yielded a variable of density for the scenarios. The other aspect of density we considered was

that of a density “bump”. A zero value for the “bump” yielded a homogeneous density, whereas a value nearing the maximum capacity for the “bump” yielded an inhomogeneous density.

4.1 Traffic Jams and Work Zones

We wanted to consider what will happen when there are situations on the road, such as: traffic jams and work zones. For a traffic jam, velocity will unexpectedly or abruptly change. Then, for a work zone, such as those on a highway, speed starts out high, say, 75mph, gradually decreases to a safe speed through the work zone, say, 25mph, then gradually returns to a high rate of speed. When these types of situations are considered, with the different types of densities, they result in the different types of scenarios that can be seen by our simulations. Our system of equations was

$$\begin{cases} v_t + vv_x & = f(\rho, v) \\ \rho_t + (\rho v)_x & = 0, \end{cases}$$

with the right-hand side of the transport equation

$$f(\rho, v) = \begin{cases} \frac{v_0 - v}{T_c} & \text{if } v_0 < v_{max} \\ \frac{v_{max} - v}{T_c} & \text{if } v_0 \geq v_{max}, \end{cases} \quad (4.1)$$

where

$$v_0(x, t) = \frac{\rho^{-1}(x, t) - L}{t_{sep}}. \quad (4.2)$$

The parameters of our simulations can be found in Table (4.1).

4.2 Scenarios

As mentioned, there were five different scenarios we considered through our simulations. Through varying velocity situations and types of densities, we were able to

Chapter 4. Modeling

Table 4.1: Table of Parameters for Simulations

Parameter	Value
Track	$L_T = 10$ miles
Grid Steps	$N = 10,000$
CFL Factor	$a = 0.1$
Spatial Grid Increment	$h = 0.001$ miles
Car Length	$L = 2.841 \times 10^{-3}$ miles
Time Characteristic	$T_c = 3.735 \times 10^{-3}$ hours
Safe Time Separation	$t_{sep} = 5.556 \times 10^{-4}$ hours

develop each type of scenario.

The first scenario had a high, yet homogeneous density of cars. The initial conditions of this scenario were:

$$v_{max}(x) = 25 + 50 \left\{ 1 - \frac{1}{\pi} [\arctan(50x - 200) - \arctan(50x - 250)] \right\}, \quad (4.3)$$

$$v(x, 0) = v_{max}(x), \quad (4.4)$$

$$\rho(x, 0) = 22. \quad (4.5)$$

Also, the cars experienced an abrupt change in velocity. This scenario was to describe cars driving on a busy highway, during a time such as the morning when people are driving to work, then suddenly encountering a velocity change. As a result, the cars could be encountering a situation similar to that of a traffic jam.

The second scenario had the same type of density, yet a smoother transition in velocity. The initial conditions of this scenario were:

$$v_{max}(x) = 23 + 52 \left\{ 1 - \frac{1}{\pi} [\arctan(10x - 37) - \arctan(10x - 53)] \right\}, \quad (4.6)$$

$$v(x, 0) = v_{max}(x), \quad (4.7)$$

$$\rho(x, 0) = 22. \quad (4.8)$$

This situation would be similar to cars driving on a highway in the morning, yet having to pass through a work zone or an accident that has been put under control.

Chapter 4. Modeling

Our third scenario was our first type of density that would be considered inhomogeneous. The initial conditions of this scenario were:

$$v_{max}(x) = 25 + 50 \left\{ 1 - \frac{1}{\pi} [\arctan(50x - 200) - \arctan(50x - 250)] \right\}, \quad (4.9)$$

$$v(x, 0) = v_{max}(x), \quad (4.10)$$

$$\rho(x, 0) = 0.2 + 22 \cdot \exp[-2(x - 2.5)^2]. \quad (4.11)$$

What is meant by inhomogeneous is that there is a high concentration or density of cars, like a “pack” of cars traveling in an otherwise lightly traveled highway. For this scenario an abrupt change in velocity occurred. This situation was to describe what happens when a special event (like a movie, concert, or sporting event), completes in the evening, then cars are leaving and suddenly get caught-up in a situation, like that of an accident or hazardous road condition.

The fourth scenario was where the density was similar to that of the third scenario, in that it was considered inhomogeneous or “pack-like”. The initial conditions of this scenario were:

$$v_{max}(x) = 23 + 52 \left\{ 1 - \frac{1}{\pi} [\arctan(10x - 37) - \arctan(10x - 53)] \right\}, \quad (4.12)$$

$$v(x, 0) = v_{max}(x), \quad (4.13)$$

$$\rho(x, 0) = 0.2 + 22 \cdot \exp[-2(x - 2.5)^2]. \quad (4.14)$$

On the other hand, there was a smooth transition in velocity. This would be like a situation of a special event completing, cars begin traveling, then encounter a construction site or work zone. This would have the cars gradually decreasing their velocity until they passed the zone, then gradually returning to their higher speed velocity.

The final scenario was a situation in which the cars had a low, homogeneous

density. The initial conditions of this scenario were:

$$v_{max}(x) = 25 + 50 \left\{ 1 - \frac{1}{\pi} [\arctan(50x - 200) - \arctan(50x - 250)] \right\}, \quad (4.15)$$

$$v(x, 0) = v_{max}(x), \quad (4.16)$$

$$\rho(x, 0) = 5. \quad (4.17)$$

Also, there was the situation of abrupt speed limit change. This was to describe the situation of a rural highway or late-night highway driving. Through the various scenarios of our simulations, the interplay of velocity and density progressed into a variety of results, which will be seen next.

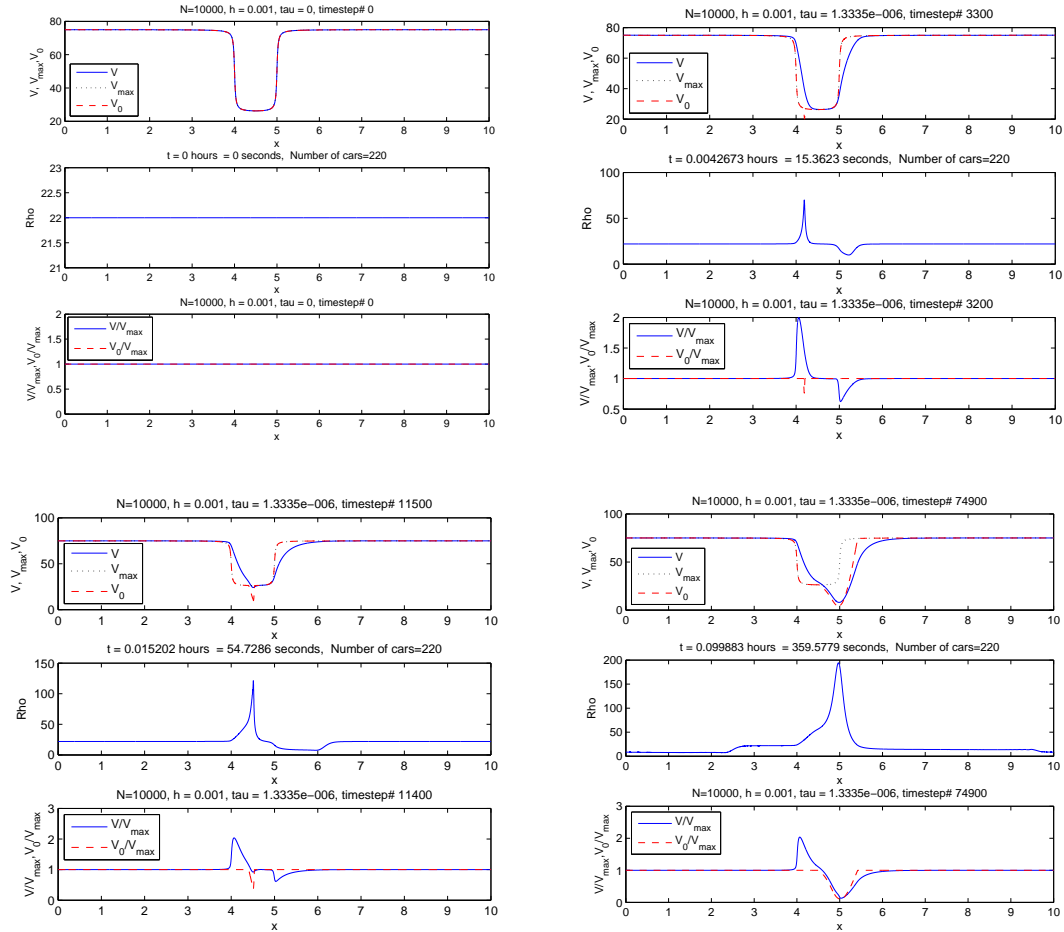
4.3 Results of Simulation

In the previous section, the five different scenarios were suggested. What follows are the results that transpired after running our simulations in Matlab. For each scenario, we took a snapshot of what took place during the initial conditions, at the time of 0 hours (which can be seen on the chart at $t = 0.000$), after the initial boundary was entered (which can be seen at about $x = 4$), the middle of our spatial interval (which can be seen at about $x = 4.5$), and at either the final time (at the time of 0.1 hours) or after the final boundary was passed (which can be seen at about $x = 5.0$), whichever came first.

As can be seen in each figure, there are four different snapshots of time for each scenario. In the titles, N is the number of grid steps, τ is the increment for the time step, and h is the increment for the grid step. For each figure, the time of each snapshot is listed under the variable t and the horizontal axis is the horizontal x -value on our track. For each snapshot on each y -axis, we show the velocity v , the speed limit or maximum velocity, v_{max} , and the desired or “safe” velocity, v_0 of the

Chapter 4. Modeling

Figure 4.1: High Homogeneous ρ , Sharp Δv Top Left: $t=0.000$; Top Right: $t=0.004$; Bottom Left: $t=0.015$; Bottom Right: $t=0.100$

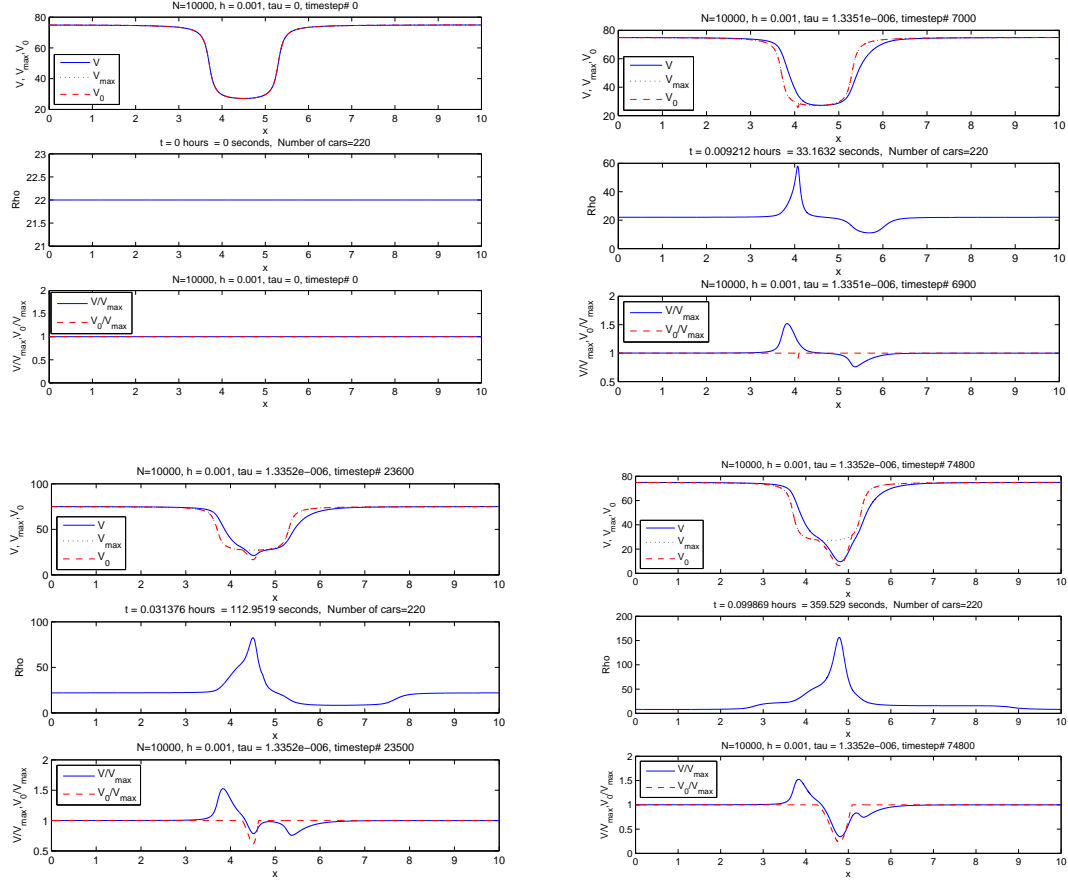


cars in the top diagram, the density, ρ , of the cars in the middle diagram, and lastly, the proportions v/v_{max} and v_0/v_{max} in the bottom diagram.

For our first scenario, our cars enter the interval of abruptly changing velocity with a high, homogeneous density. To achieve this, the lower limiting density was set close to the maximum capacity at 22 cars per mile for the initial conditions. Then, since the change of velocity is sharp, we begin to see a spike for the desired velocity below the speed limit after entering the interval. The average velocity is above the

Chapter 4. Modeling

Figure 4.2: High Homogeneous ρ , Smooth Δv Top Left: $t=0.000$; Top Right: $t=0.009$; Bottom Left: $t=0.031$; Bottom Right: $t=0.100$



speed limit at this time, then becomes only slightly below the speed limit in the middle of the interval. The safe velocity has an even sharper spike in the middle of the interval. Then, at the end of the interval, when the speed limit is increased abruptly, both the desired and average velocities are considerably below the speed limit. (See Figure 4.1)

For the second scenario, our density of cars is also homogeneous and high as they enter the interval of changing velocity. So, the initial conditions are similar to the first scenario. Since the change of velocity is more gradual after entering the

Chapter 4. Modeling

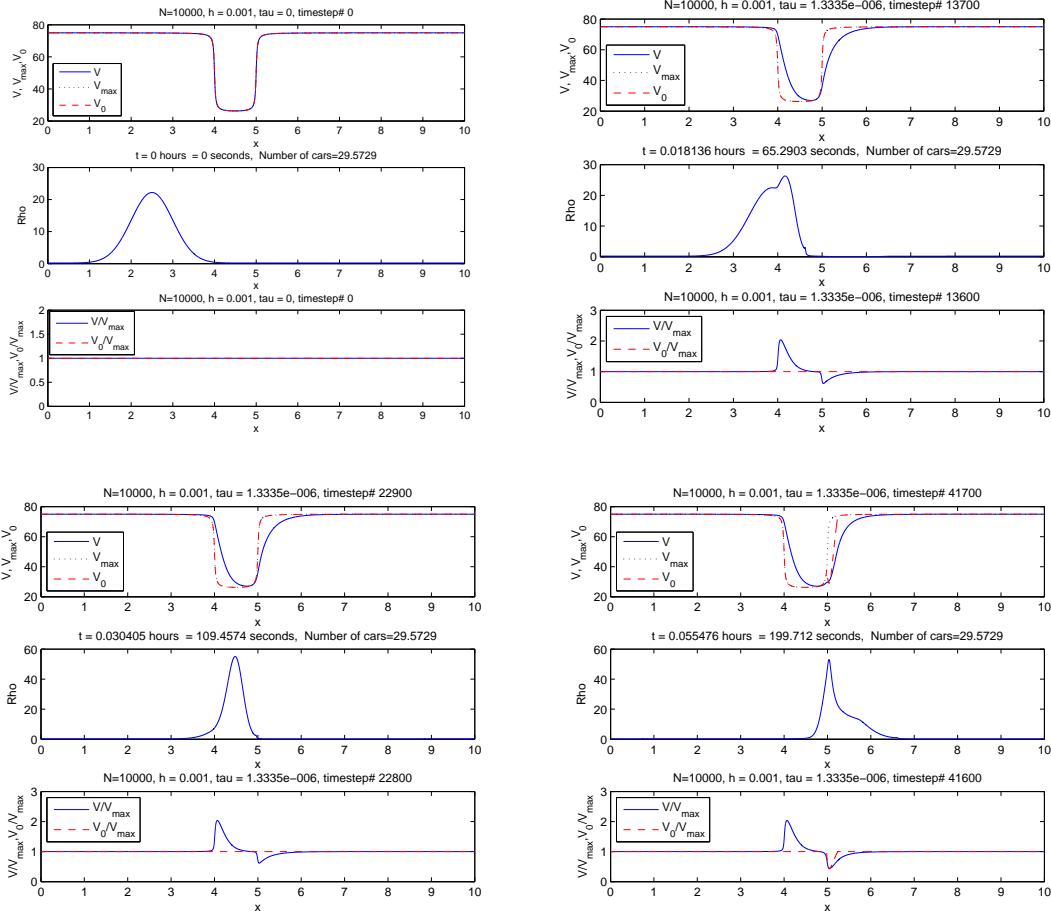
interval (compared to the first scenario), we see the desired velocity begin to be below the speed limit. Whereas, the average velocity is only slightly above the speed limit compared to the first scenario. The safe velocity being below the speed limit becomes pronounced as the cars progress to the middle of the interval. This is also where the average velocity is below the speed limit and even *more* pronounced than in the first scenario. Then by the end of the interval, both the desired and average velocities are considerably below the speed limit. Also, with the time frame used, through the sixth minute (or 100 seconds), this scenario of cars does not appear to have made it through the end of the interval (at the fifth mile). Yet, the levels are not as pronounced as the last snapshot of the first scenario. (See Figure 4.2)

We have a high, inhomogeneous density for the third scenario as the cars enter the interval. In order to achieve this, we set our initial conditions to have a lower limiting density close to zero (but slightly above zero to avoid negative densities) and the density “bump” nearing the maximum capacity. After entering the interval, we do not see much of a difference in the desired and maximum (speed limit) velocities, whereas the average velocity is markedly above the speed limit. We do not see much of a change in the middle of the interval for the desired velocity, but the average velocity is more coincident with the speed limit. Then the speed limit abruptly changes back to the high velocity and we see a spike below the speed limit for the desired velocity and the average velocity is now below the speed limit, although just slightly. Noticeably different is that the cars pass through the interval in almost half of the time for the third scenario than in either the first or second scenarios. (See Figure 4.3)

For the fourth scenario, the density of cars is high, yet inhomogeneous, similar to the initial conditions of the third scenario. Yet, the cars begin to enter the interval of a more smoothly changing speed limit. After entering the interval we see that the speed limit and desired velocity are similar and the average velocity is not much

Chapter 4. Modeling

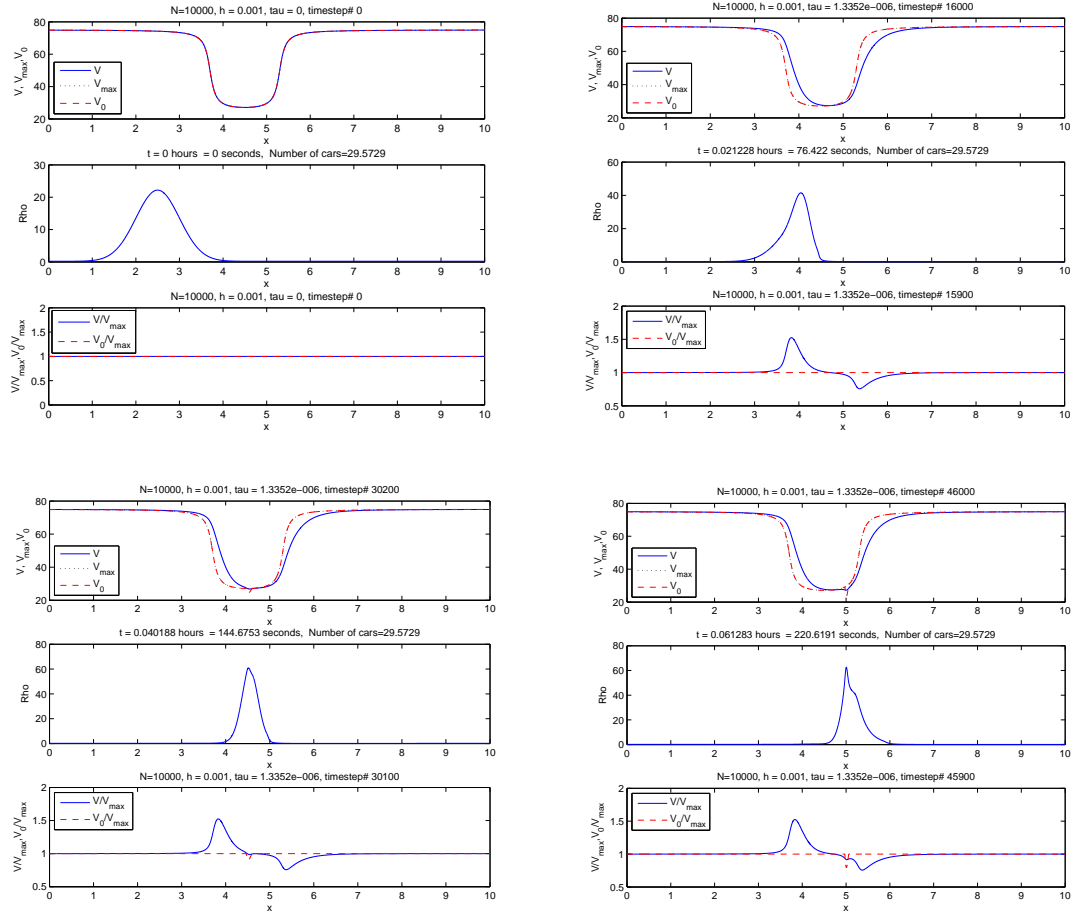
Figure 4.3: High Inhomogeneous ρ , Sharp Δv Top Left: $t=0.000$; Top Right: $t=0.018$; Bottom Left: $t=0.030$; Bottom Right: $t=0.055$



higher than the speed limit, especially compared to the third scenario. In the middle of the interval we see that the desired velocity has a small dip below the speed limit, although now the average velocity is about the same as the speed limit. Then, as in the third scenario, the average velocity is below the speed limit, yet the desired velocity has shifted forward with a more pronounced, yet smooth, level below the speed limit as the cars pass through the end of the interval. Also, we see that the time for the cars to complete the interval takes longer, compared to the third scenario (yet still, about two thirds as fast as either the first or second scenarios). (See Figure

Chapter 4. Modeling

Figure 4.4: High Inhomogeneous ρ , Smooth Δv Top Left: $t=0.000$; Top Right: $t=0.021$; Bottom Left: $t=0.040$; Bottom Right: $t=0.060$

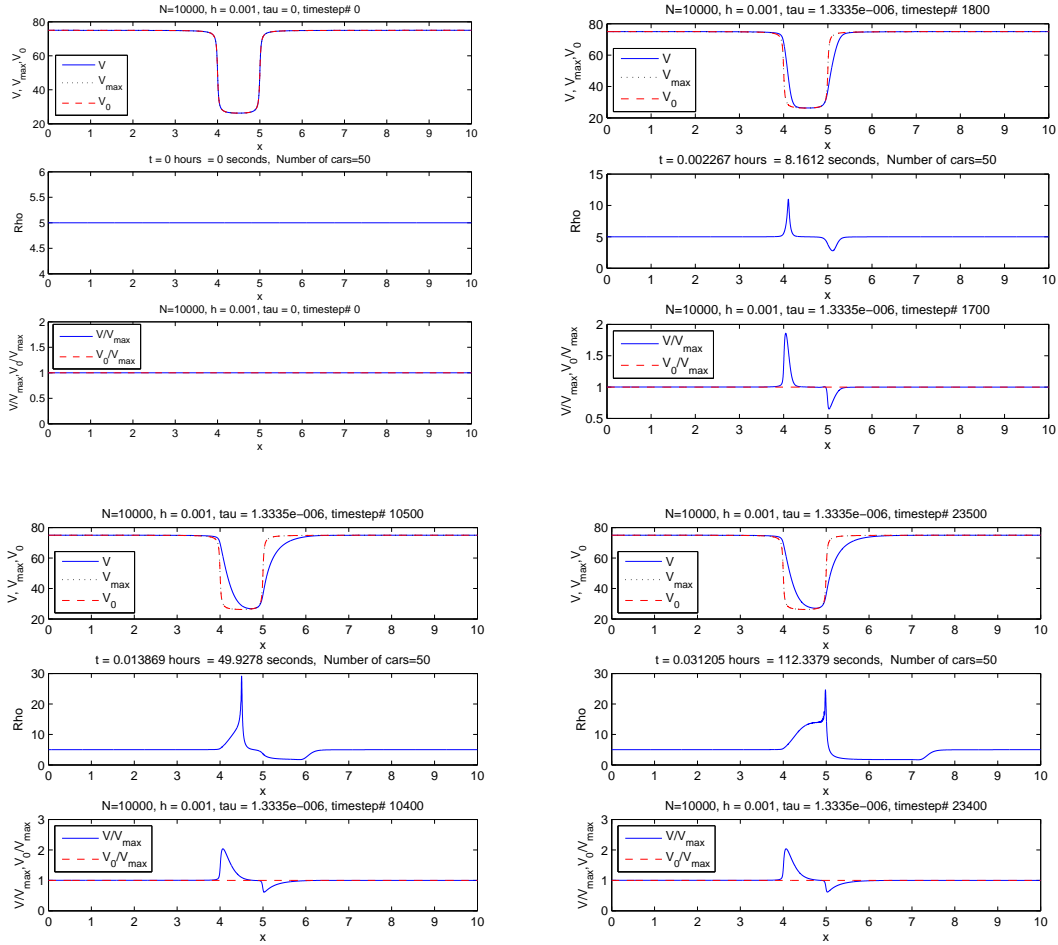


4.4)

For the fifth and final scenario we have a low, homogeneous density as we enter the interval of a sharply changing speed limit. In order to achieve this type of density, the lower limiting density is set to slightly lower than one fourth of the maximum capacity and the “bump” is set to zero for the initial conditions. After entering the interval, the desired velocity is the same as the speed limit, yet the average velocity is above the speed limit. In the middle of the interval, we do not have any change, as

Chapter 4. Modeling

Figure 4.5: Low Homogeneous ρ , Sharp Δv Top Left: $t=0.000$; Top Right: $t=0.002$; Bottom Left: $t=0.014$; Bottom Right: $t=0.031$



desired and average velocity is the same as it relates to the speed limit. After passing through the interval, both the desired and average velocity appear to be coincident with the speed limit. What is markedly different in this scenario compared with the other scenarios is how fast the cars pass through the interval. The cars pass through the interval in about two thirds of the time as the next fastest scenario (that being the third scenario). (See Figure 4.5)

Chapter 5

Conclusion

In terms of the first two scenarios, where the cars have a high, homogeneous density, during the middle of the interval it is as if the rapidly changing velocity scenario had an unexpected drop in the desired velocity compared to the second scenario. Also, when the speed limit gradually changed, it is as if the desired and average velocities have already accounted for road conditions, and so, no shock to the system is seen. For the third scenario, in the end, the desired velocity has a spike below the speed limit compared to the smoother, continuing nature of the shape of the desired velocity curve below the speed limit of the fourth scenario. It is as if the drivers were able to make a more comfortable adjustment in controlling the velocity of their car. Then, in the last scenario, the overriding quality of the cars is that there is a low homogeneous density. So, in this case, it did not seem to matter if there was a sharp change in the speed limit, since the desired or safe velocity was consistently the same as the speed limit (and actually cannot go any higher, based on our definition of desired velocity) throughout the entire interval. We also see that the average velocities are not as far above the speed limits for scenarios where there is a gradual change of the speed limit (scenarios two and four) compared to a more abruptly changing speed limit (scenarios one and three). Through our simulations

Chapter 5. Conclusion

and analysis of results, we are led to conclude that in terms of being able to adjust to road conditions, a gradual change of speed limit benefits drivers compared to a more abruptly changing one.

References

- [1] Evan Ackerman, *Study: Intelligent cars could boost highway capacity by 273%*, 2012. <http://spectrum.ieee.org/automaton/robotics/artificial-intelligence/intelligent-cars-could-boost-highway-capacity-by-273>.
- [2] Hirotashi Hanaura and Takashi Nagatani and Katsunori Tanaka, *Jam formation in traffic flow on a highway with some slowdown sections*, *Physica A* **374** (2006), 419–430.
- [3] J. G. Charney, R. Fjörtoft, and John von Neumann, *Numerical integration of the barotropic vorticity equation*, *Tellus* **2** (1950), 237–254.
- [4] M. R. Flynn, A. R. Kasimov, J. C. Nave, R. R. Rosales, and B. Seibold, *Self-sustained nonlinear waves in traffic flow*, *Physical Review E* **79** (2009), 056113.
- [5] Hyun Keun Lee and Beom Jun Kim, *Dissolution of traffic jam via additional local interactions*, *Physica A* **390** (2011), 4555. arXiv: 1109.2191v1.
- [6] New Mexico’s Department of Transportation Motor Vehicle Division, *Driver handbook drivers license manual dmv-new mexico*, 2012. <http://www.mvd.newmexico.gov/sitecollectiondocuments/assets/dlm.pdf>.
- [7] R.D. Richtmyer and K.W. Morton, *Difference methods for initial value problems*, 2nd ed., Wiley-Interscience, New York, 1967.
- [8] John C. Strikwerda, *Finite difference schemes and partial differential equations*, 2nd ed., Wadsworth & Brooks/Cole, 1989.

REFERENCES

- [9] Patcharinee Tientrakool, Ya-Chi Ho, and Nicholas F. Maxemchuk, *Highway capacity benefits from using vehicle-to-vehicle communication and sensors for collision avoidance*, 2011.
- [10] G. B. Whitham, *Linear and nonlinear waves*, John Wiley & Sons, 1999.
- [11] Lisa Zyga, *Removing ‘black sheep’ could make internet run more efficiently*, 2012.
<http://phys.org/news/2012-02-black-sheep-internet-efficiently.html>.